J Vis (2019) 22:1071–1080
https://doi.org/10.1007/s12650-019-00596-z

REGULAR PAPER

Łukasz Jan Kapusta · Ireneusz Pielecha · Krzysztof Wisłocki · Andrzej Teodorczyk

n-Hexane injection into high-temperature and high-pressure environments

Received: 12 February 2019 / Revised: 20 April 2019 / Accepted: 9 August 2019 / Published online: 24 August 2019

Abstract In this study, the process of *n*-hexane spray formation was investigated under a wide range of environmental conditions. The main aim of this research was to determine whether the global and visual properties of *n*-hexane spray change when the back pressure exceeds the critical pressure of the injected liquid. For this purpose, the liquid length and the boundary profile between the spray and surrounding air obtained by high-speed imaging of the Mie scattering signal were used. A major advantage of this work is that besides measuring global spray parameters, it provides quantitative analysis of the visual properties of the spray images; thus, the image analysis is not limited to qualitative visual impression. The results obtained in this study showed no step change in liquid length in terms of exceeding the critical parameters. Although qualitatively the boundary between the injected liquid and the surrounding gas seemed to become smoother in high-pressure and high-temperature conditions, the qualitative analysis did not support this observation.

Keywords Injection · Rapid compression machine · RCM · Spray · Supercritical mixing · Mie scattering

List of symbols

l_l	Liquid length
p_{cr}	Critical pressure
p_{gas}	Gas pressure at start of injection
p_r	Reduced pressure
RCM	Rapid compression machine
SOI	Start of injection
T_{cr}	Critical temperature
T_{gas}	Gas temperature at start of injection
T_{inj}	Temperature of injected liquid
T_r	Reduced temperature

Ł. J. Kapusta (✉) · A. Teodorczyk
Institute of Heat Engineering, Faculty of Power and Aeronautical Engineering, Warsaw University of Technology, Nowowiejska 21/25, 00-665 Warsaw, Poland
E-mail: Lukasz.Kapusta@pw.edu.pl
Tel.: +48 22 234 52 41

I. Pielecha · K. Wisłocki
Faculty of Transport Engineering, Poznan University of Technology, Piotrowo 3, 60-965 Poznan, Poland

1 Introduction

Injection into environments of pressure and temperature exceeding fuel critical parameters in terms of hydrocarbon fuels has become of high interest very recently. However, the supercritical mixing has been studied previously in terms of injection of liquid propellants and oxidizers in rocket propulsion (Chehroudi et al. 2002; Schmidt et al. 2002; Zong and Yang 2006; Segal and Polikhov 2008; Roy and Segal 2010). In many studies, researchers working on this topic linked the change in mixing behaviour to approaching and exceeding critical parameters of the injected liquid (Mayer et al. 1998; Chehroudi et al. 2002; Oefelein 2006; Oschwald et al. 2006; Zong and Yang 2006; Segal and Polikhov 2008; Rachedi et al. 2010; Roy and Segal 2010).

Mayer et al. (1998), studying liquid propellant injection into high-pressure environments, observed a remarkable difference between spray formation at sub- and supercritical pressure. Chehroudi et al. (2002) noticed a lack of any visual detection of drops when the back pressure approached and exceeded the critical pressure of the injectant. They had a visual impression of the gaseous jet and noticed the inhibition of the transition into the full atomization regime. Both research teams Mayer et al. (1998) and Chehroudi et al. (2002) concluded that the observed difference in the visual impression of the jet was caused by the fact that the surface tension approaches zero when the fluid pressure approaches and exceeds the critical value.

Segal and Polikhov (2008) concluded that transitional and supercritical mixing can be observed when only the temperature or the pressure is higher than the critical value of the injected liquid. They emphasized, however, that this observation is valid only when the second parameter is not substantially lower than the critical parameter of the injected liquid.

Experiments made by Rachedi et al. (2010) for a swirl injector showed that the behaviour of a supercritical hydrocarbon jet and a supercritical CO_2 jet was similar in most investigated aspects. Dahms et al. (2013) showed that the mixing behaviour of a hydrocarbon fuel (*n*-dodecane) changes when the temperature of the surrounding gas exceeds the fuel's critical temperature. They noticed that for higher temperatures, darker regions signifying light scatter and extinction by liquid were still present in some locations. However, the transition from liquid to gaseous state appeared to be much smoother than at the low-temperature condition. They stated that while the fuel vaporization rates increased because of higher gas temperature, total vaporization of the liquid could not explain the lack of ligaments or droplets observed for the 900 K condition.

Dahms and Oefelein (2013, 2015) suggested that exceeding supercritical parameters of the injected liquid may not be sufficient for the mixing transition. In their work (Dahms and Oefelein 2013), their calculations revealed that enthalpy of hot surrounding gases is not sufficient to heat up the gas–liquid interface to its critical temperature. They suggested that the transition between two-phase and single-phase interface dynamics is not necessarily induced by diminished surface tension forces alone (Dahms and Oefelein 2013). Instead of reaching the injectant critical parameters' criterion, they proposed a criterion of a Knudsen number lower than 0.1 for supercritical mixing. They defined the Knudsen number as the ratio of two-fluid interface thickness to the mean free path. Their considerations were focused on multi-component fluids, where in most cases the surface tension cannot be neglected. In single-component liquids, the surface tension may be neglected when the critical pressure of the liquid is exceeded.

The other important issue is the fact that immediately after the injection, a part of the injected liquid mixes with the surrounding gas and the properties of the mixture become completely different. The same researchers in the same study (Dahms and Oefelein 2013) stated that mixtures of a mixture fraction below 0.5 can be described as an ideal gas and the effects of real fluid behaviour do not play a role. Nevertheless, one needs to take into account that the process of such a mixture formation may be affected by real fluid behaviour.

Dahms and Oefelein (2015) noticed that mixing depends on the distance from the outlet of the nozzle. They suggested that the association of the continuum regime, where statistical fluctuations are negligible, is only valid in the dilute-gas regime but not in the dense-fluid regime associated with high-pressure liquid injection processes (Dahms and Oefelein 2015). Most recently Crua et al. (2017) confirmed the occurrence of the transition from classical liquid–gas mixing to mixing where surface tension forces diminish at high-pressure and high-temperature conditions. They, however, noticed that the transition to diffusive mixing does not occur instantaneously, but after some time when the liquid structures are surrounded by the hot ambient gas. They proposed a phenomenological model based on critical properties of the injected liquid to predict the transition from classical liquid–gas mixing to diffusive mixing.

In our previous study on *n*-hexane spray auto-ignition and combustion (Kapusta et al. 2016), depending on the conditions, a different visual impression of the spray was noticed, even though all cases were within the range of subcritical mixing according to the model proposed by Crua et al. (2017). In their study, long-distance microscopy with backlight illumination was used, capable of resolving a single droplet, which makes their approach very accurate in terms of formulating a criterion for the mixing transition. However, there is still a question of what this criterion has to do with macroscopic observations, especially some of those which have led to conclusions on the mixing transition close to critical point parameters, while the criterion formulated by Crua et al. (2017) is far from a critical point.

Therefore, in this study, we provide macroscopic spray visualization using high-speed imaging of Mie scattering, which is a well-accepted method for global spray visualization (Chen et al. 2014; Sun et al. 2018). It needs to be emphasized that this study is not limited to qualitative analysis based on the visual impression of the sprays, but also provides quantitative analysis of the spray-gas boundary. Moreover, we combine these observations with a liquid length analysis, in order to verify any possible link between visual impression and global spray properties.

2 Experimental set-up

The research was conducted on the pneumatically driven rapid compression machine (RCM) with constant compression ratio achieved by a mechanical coupling with rotating counterweights. The experimental set-up is shown in Fig. 1.

The compression ratio in this research was set to 9. The RCM piston stroke was 81 mm, while the cylinder bore was 80 mm. The piston speed was around 1 m/s (depending on the air pressure under the piston).

In this study, a Siemens VDO piezoelectric gasoline outwards opening pintle injector was used. The injector was of a standard design without an inside swirl. The maximum needle lift was 40 μm (Gavaises et al. 2006), and the static flow rate was 36 g/s (Warnecke et al. 2006). Detailed geometrical data of the injector are shown in Gavaises et al. (2006). The injector was located in centre of the RCM head (Fig. 1) in order to inject the fuel into the centre of the combustion chamber where the thermodynamic conditions are least affected by the walls and the airflow acts symmetrically on the spray.

The in-cylinder pressure was measured by an AVL GM11D piezoelectric pressure transducer and an AVL IndiCom 621 data acquisition system. The spray was observed using a LaVision HSS5 high-speed camera at a frame rate of 20,000 fps with a resolution of 384 × 304 pixels. In order to avoid signal attenuation leading to non-uniform spray visualization (Chen et al. 2014), instead of light-sheet imaging, a global illumination was applied. The sprays were illuminated through the window in the piston by an external source of light (two halogen lights—500 W each), and the back-scattered light was recorded by the camera using the same window and mirror (Fig. 1).

In this study, *n*-hexane was used to reproduce conditions from the work of Kapusta et al. (2016). According to Linstrom and Mallard (2001), critical point parameters of *n*-hexane are: 507.6 ± 0.5 K and 3.02 ± 0.04 MPa. In all cases, injection pressure was the same at 20 MPa. The liquid temperature was set to 293, 323, 343, 373 and 423 K. Ambient air was used as a working gas. The air pressure at the start of injection varied from 0.36 to 7.06 MPa, while the temperature ranged from 450 to 1100 K. Note that the air

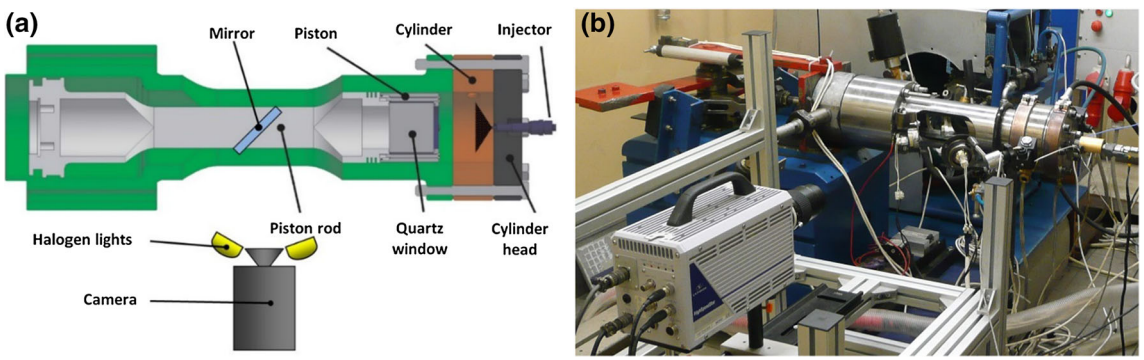

Fig. 1 Experimental set-up: **a** schematic diagram; **b** photograph

temperatures at start of injection (SOI) were calculated based on an assumption of a uniform temperature and a constant polytropic coefficient.

3 Results and discussion

For every case, a set of frames was collected. For the first step of the image processing, the background image was subtracted from raw images. In Fig. 2, selected frames for four selected cases after background subtraction (for supercritical, around critical and subcritical pressure) were presented. The temperature of the gas at SOI in these cases was above the critical temperature of *n*-hexane. The *n*-hexane initial temperature in all four cases was of 423 K. The parameters of air in the chamber at start of injection were provided by means of reduced pressure—p_r, and reduced temperature—T_r, which are the parameters normalized by *n*-hexane critical parameters according to Eqs. 1 and 2, respectively.

$$p_r = \frac{p_{gas}}{p_{cr}} \tag{1}$$

where p_{gas} is the gas pressure inside the chamber at start of injection, while p_{cr} is the critical pressure of *n*-hexane

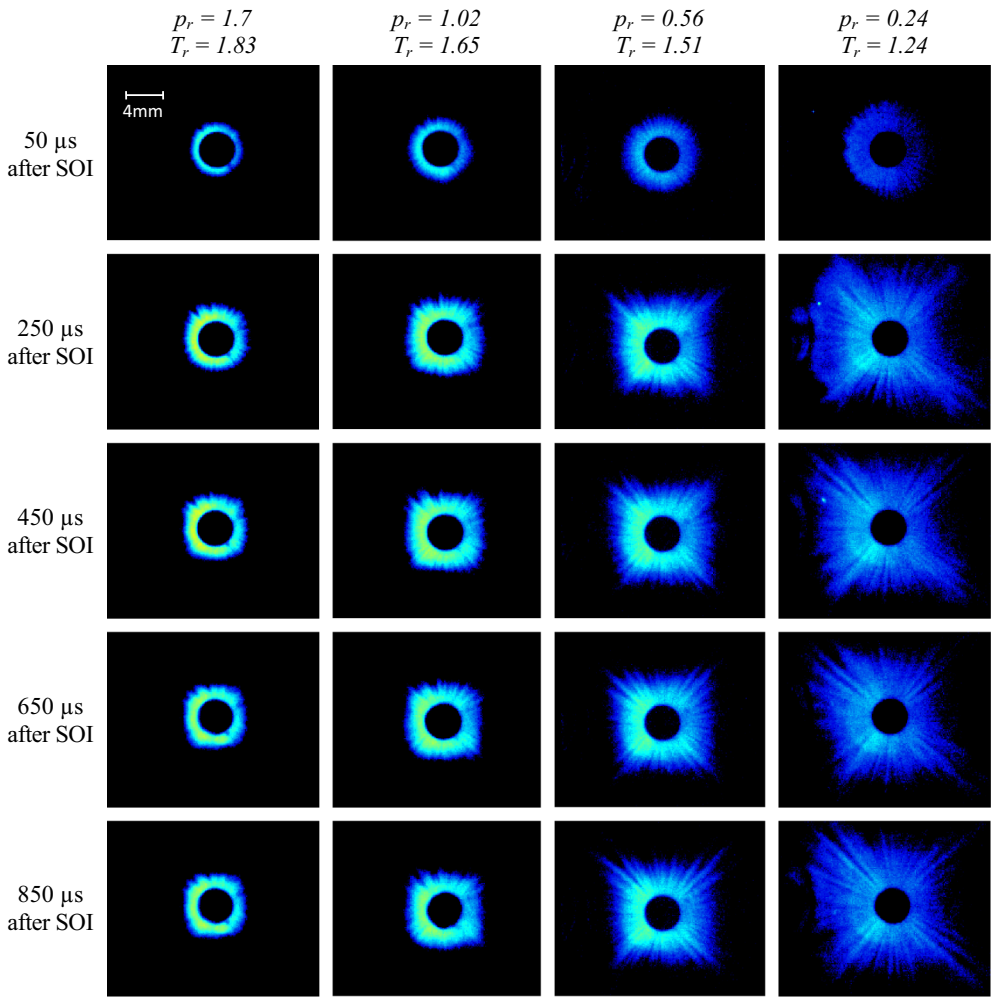

Fig. 2 View of the *n*-hexane spray for two extreme cases; p_r and T_r stand for reduced pressure and reduced temperature, respectively—the parameters normalized by *n*-hexane critical parameters

$$T_r = \frac{T_{gas}}{T_{cr}} \tag{2}$$

where T_{gas} is the gas temperature inside the chamber at start of injection, while T_{cr} is the critical temperature of *n*-hexane.

The images presented in Fig. 2 show the initial stage of injection as well as fully developed sprays. One can clearly see that the major difference in spray shape between the cases is the liquid length. It might be argued that the visual impression of the sprays is also different. The boundary between the light area (representing the injected liquid) and the dark area (representing the surrounding gas) seems to be more diffusive for the high-pressure and high-temperature case. In order to verify the visual impression quantitatively, all the acquired images were further processed using LaVision DaVis v8.3 software. The acquired frames (after background subtraction) were used to determine the liquid length evolution and its circumferential distribution (around the injector axis). To determine the liquid length, the intensity threshold was set to 25 counts. The circumferential distribution of the gas–liquid boundary was determined every two degrees around the injector axis as shown in Fig. 3 (by white dots).

Based on the obtained results, the average liquid length for each image was calculated. It was taken into account that the visualized spray is a projection on a camera matrix, and thus, the presented values are higher than directly seen in the images. The evolution of the spray-gas boundary (only for selected frames: 0.05, 0.1, 0.2, 0.4 and 0.8 ms after SOI) is shown in Fig. 4a. In order to measure the circumferential distribution of the liquid length (i.e. dispersion from the average around the injector axis), the standard deviation was calculated. The graph showing the temporal evolution of the average liquid length and the standard deviation of the liquid length for one of the cases (T_{inj} = 373 K; p_{gas}= 0.84 MPa; T_{gas} = 737 K) is presented in Fig. 4b.

The average liquid length evolution presented in Fig. 4b clearly shows that after initial rapid growth, the liquid length becomes relatively constant (with some oscillations). It comes from the fact that at a certain time after SOI, the mass of the liquid, which changes its state to vapour or supercritical per unit of time, becomes equal to the mass flow rate of the injected liquid. The parameters of the sprays for their developed stages were calculated in order to compare the sprays from different environments. Equation (3) is used to determine the time-average liquid length for developed sprays.

$$\overline{l_l} = \sum_{i=11}^{n} \frac{l_l(i)}{n} \tag{3}$$

where i is the frame number (frame number 11 was obtained at 0.5 ms after SOI); n is the total number of frames collected for a certain case; and l_l is the average liquid length for one frame. The time-average liquid length for the developed sprays for all cases (including different liquid temperatures—T_{inj}) for corresponding chamber conditions at SOI is shown in the graph in Fig. 5.

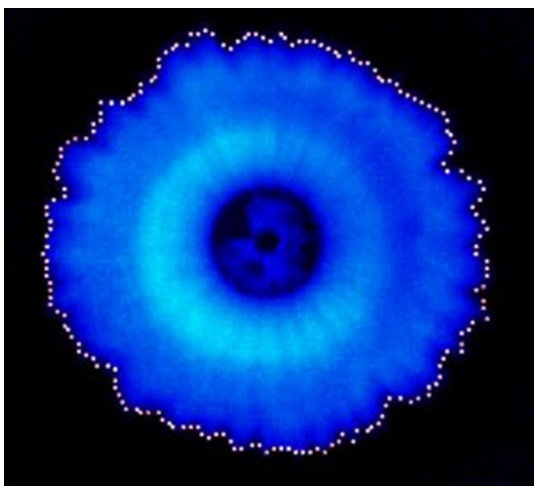

Fig. 3 Determination of the liquid length around the injector axis

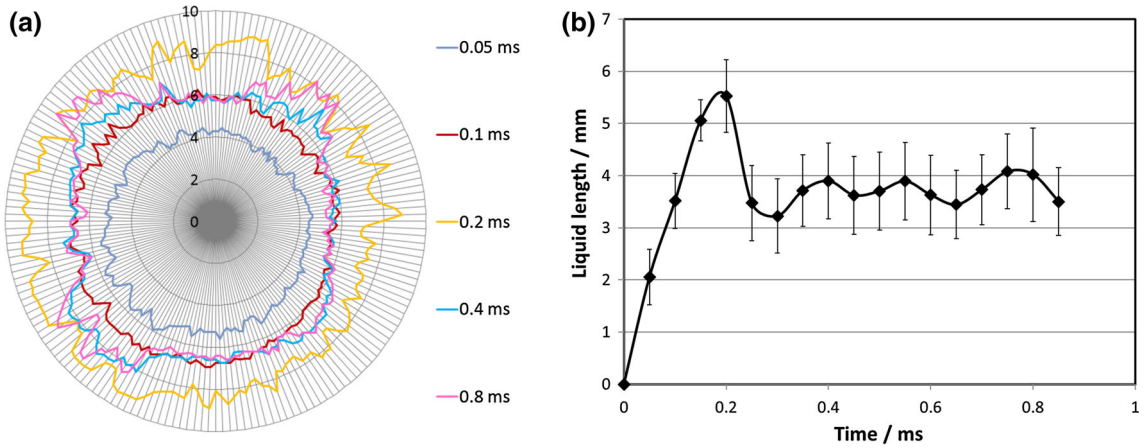

Fig. 4 **a** Determined liquid length around injector axis (in mm) for selected frames for T_{inj} = 423 K, p_{gas}= 3.07 MPa, T_{gas} = 840 K; **b** average liquid length and standard deviation of liquid length (shown as error bars) for each frame for the same case

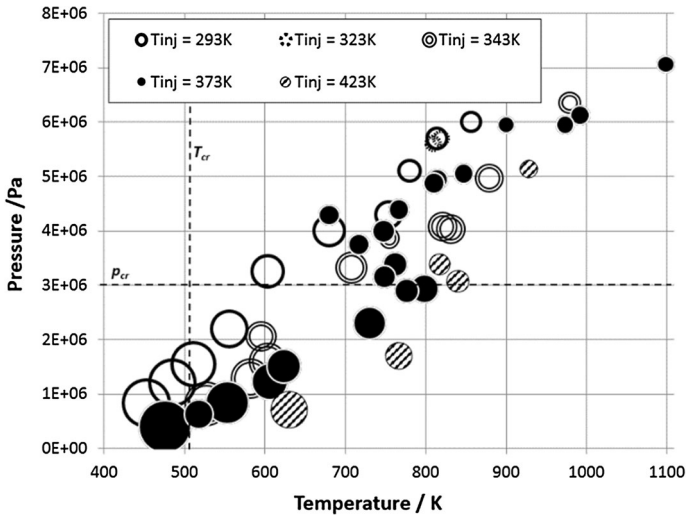

Fig. 5 Time-average liquid length (represented by the size of the circles) of developed sprays ($t \geq 0.5$ ms); the size of the smallest circle corresponds to the value of 2.17 mm, while the size of the biggest circle to the value of 20.51 mm

The time-average liquid length (i.e. average liquid length of a developed spray) decreases with increased pressure and temperature. It might be speculated whether exceeding the critical pressure has a stronger effect on liquid length than exceeding the critical temperature. However, if the cases for constant fuel temperature are considered, then the change in liquid length appears to be gradual. This shall be associated with increased density of the air inside the chamber, which increases along with pressure and temperature with piston movement. As shown previously by other researchers, gas density is one of the crucial parameters in terms of spray development for cylindrical nozzles (Hiroyasu and Arai 1990; Siebers 1999; Dos Santos and Le Moyne 2011; Ghurri et al. 2012) as well as for hollow-cone injectors (Dong et al. 2013). Moreover, as shown in Fig. 5, there is no specific change in time-average liquid length around critical pressure or temperature, which could be associated with a sudden change in the mixing process.

As for the macroscopic boundary between the spray and the surrounding gas, the standard deviation of liquid length (around the injector axis) calculated directly could not be associated with the roughness of the spray-liquid boundary. The standard deviation is affected not only by the roughness of this boundary but also by the eccentricity of the spray. Therefore, in order to quantitatively represent the roughness of the spray-gas boundary, the new average circle was fitted by the least squares method (Fig. 6) as described by Shakarji (1998).

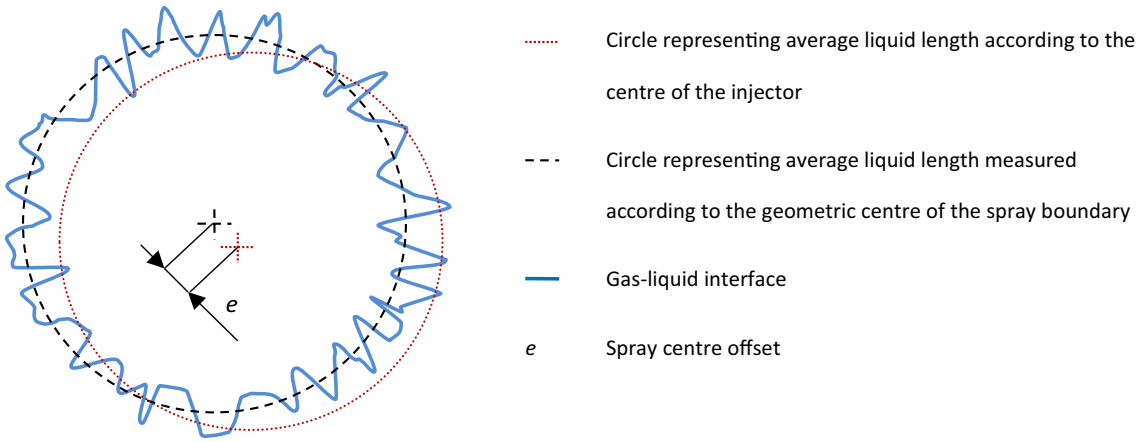

Fig. 6 Schematic correction of the spray centre

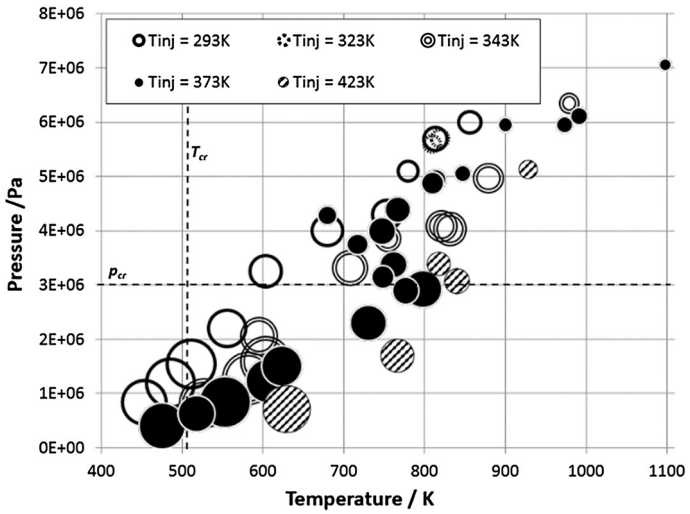

Fig. 7 Standard deviation of liquid length (represented by size of the circles) of developed sprays ($t \geq 0.5$ ms) calculated from the new spray centre; the size of the smallest circle corresponds to the value of 0.18 mm, while the size of the biggest circle to the value of 2.6 mm

After the spray centre and radius correction, the standard deviation of the liquid length (Fig. 7) became more representative of the roughness of the spray-gas boundary. Note that the standard deviation of the liquid length (around the centre of the spray) for a single case (single point in Fig. 7) was calculated for all frames recorded from 0.5 ms after SOI.

The standard deviation of the liquid length of the developed sprays ($t \geq 0.5$ ms) calculated from the corrected spray centre and radius significantly decreases when pressure and temperature in the RCM are increased. This, however, can be associated with much lower liquid length for high-pressure and high-temperature conditions (see Fig. 5). Therefore, the standard deviation of the liquid length was normalized by the radius of the circle fitted to the collected points representing the gas–liquid boundary (black dash line in Fig. 6). The normalized values of the standard deviation of the liquid length for the corrected spray centre are shown in Fig. 8.

Although the relative standard deviation of the liquid length of the developed sprays ($t \geq 0.5$ ms) calculated from the new spray centre (Fig. 8) does not decrease as much as the standard deviation (Fig. 7) when pressure and temperature in the RCM are increased, the values obtained for the highest pressures and temperatures tend to be smaller. The circle representing the smallest value of relative standard deviation is indeed recorded for the highest pressure and temperature. Moreover, it was just over the limit for transitional mixing according to the model proposed by Crua et al. (2017). It is, however, difficult to explain the weak

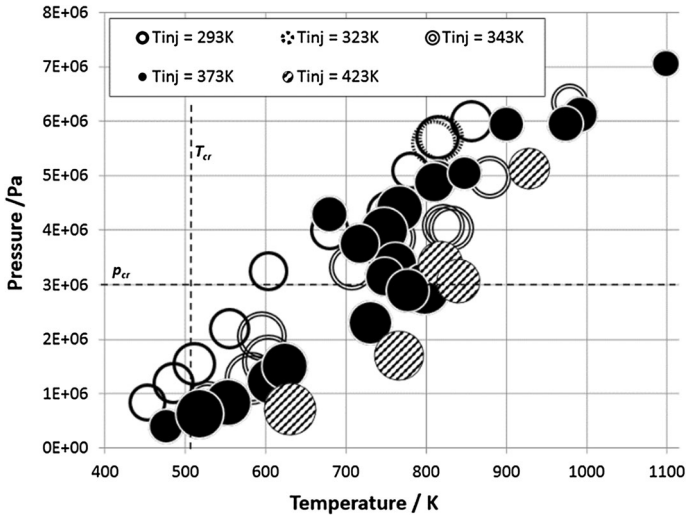

Fig. 8 Relative standard deviation of liquid length (represented by size of the circles) of developed sprays ($t \geq 0.5$ ms) calculated from the new spray centre; the size of the smallest circle corresponds to the value of 0.06, while the size of the biggest circle to the value of 0.22

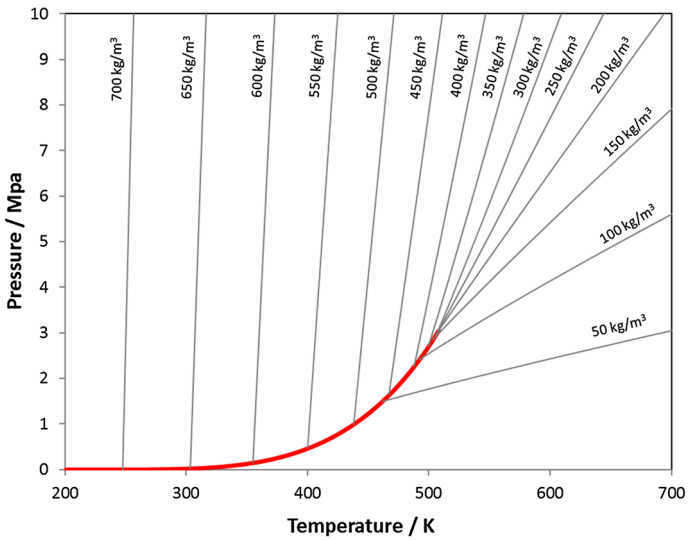

Fig. 9 Vapour pressure of *n*-hexane (red bold line) and iso-line of density (grey thin lines)

tendency of this parameter to decrease, while pressure and temperatures become higher. It does not need to be associated with mixing transition, but can be also caused by the higher heat transfer and vaporization rate stopping spray fragments, which are growing faster, from penetrating further. Another important aspect to consider is that the real gas effects are especially strong in the vicinity of the critical point. When the temperature is higher than critical, and pressure is close to the critical pressure, then the small change in pressure causes rapid changes in density and vice versa, as shown in Fig. 9. In the cases considered in the study, none of them were close to the critical point (as seen in Figs. 5, 7 and 8).

Another factor which may affect the spray-gas boundary and shall be taken into account is the boundary representation by the raster image. When the differences between spray fragments penetrating for short and for long distances become smaller, the effects of pixel resolution become more important and may lead to blurring of the spray-gas boundary. This effect is magnified when the liquid length is shorter. Then, also the average boundary of the spray is represented by the smaller number of pixels (smaller circle). The observed blurred spray-gas boundary in turn may be misinterpreted and associated with the effect of diffusive mixing, as shown in Fig. 2.

4 Conclusions

The observation of the spray formed by *n*-hexane injected into various environments made in this study clearly showed that the spray changes significantly with an increase in back pressure and temperature of the surrounding gas. The major difference was related to liquid length. However, the boundary between the spray and the surroundings seemed to be smoother and more diffusive in higher-pressure and higher-temperature conditions.

The dispersion of the spray-gas boundary (i.e. circumferential distribution of the liquid length) measured by means of the standard deviation of the liquid length quantitatively confirmed this observation. However, after normalizing the standard deviation of the liquid length, this trend became much weaker and difficult to associate with the mixing transition due to several reasons:

- In high-temperature environments, higher heat transfer and vaporization rate stop the spray fragments, which are moving faster, from penetrating much further;
- Smaller differences between spray fragments penetrating for short and for long distances caused by a decreased maximum liquid length in high-pressure conditions may become more blurred due to pixel resolution effects. This phenomenon is additionally enhanced by the arrangements as studied here; where with a decreased liquid length, the boundary between gas and spray is also decreased and represented by a lower number of pixels;
- Only one measurement considered here was slightly above the condition for transitional mixing formulated by other researchers for single-component hydrocarbon fuel.

In general, taking into account the quantitative results presented in this study and the findings of other researchers, it may be concluded that a change in mixing appearance with an increase in surrounding pressure and temperature in a supercritical regime is observed. However, it is not necessarily associated with real gas effects, but maybe caused by the images' visual properties, most probably coupled with other factors like a high evaporation rate in high-temperature conditions.

Acknowledgements This study was funded by the National Science Centre of Poland within the framework of the OPUS programme under Agreement UMO-2012/07/B/ST8/03632.

References

Chehroudi B, Talley D, Coy E (2002) Visual characteristics and initial growth rates of round cryogenic jets at subcritical and supercritical pressures. Phys Fluids 14(2):850–861. https://doi.org/10.1063/1.1430735

Chen H, Hung DLS, Xu M (2014) A dynamic thresholding technique for extracting the automotive spark-ignition direct-injection pulsing spray characteristics. J Vis 17:197–209. https://doi.org/10.1007/s12650-014-0203-8

Crua C, Manin J, Pickett LM (2017) On the transcritical mixing of fuels at diesel engine conditions. Fuel 208:535–548. https://doi.org/10.1016/j.fuel.2017.06.091

Dahms RN, Oefelein JC (2013) On the transition between two-phase and single-phase interface dynamics in multicomponent fluids at supercritical pressures. Phys Fluids 25(9):092103. https://doi.org/10.1063/1.4820346

Dahms RN, Oefelein JC (2015) Non-equilibrium gas-liquid interface dynamics in high-pressure liquid injection systems. In: Proceedings of the Combustion Institute. The Combustion Institute, vol 35(2), pp 1587–1594. https://doi.org/10.1016/j.proci.2014.05.155

Dahms RN, Manin J, Pickett LM, Oefelein JC (2013) Understanding high-pressure gas-liquid interface phenomena in diesel engines. In: Proceedings of the Combustion Institute. The Combustion Institute, vol 34(1), pp 1667–1675. https://doi.org/10.1016/j.proci.2012.06.169

Dong Q, Ishima T, Kawashima H, Long W (2013) A study on the spray characteristics of a piezo pintle-type injector for DI gasoline engines. J Mech Sci Technol 27(7):1981–1993. https://doi.org/10.1007/s12206-013-0510-3

Dos Santos F, Le Moyne L (2011) Spray atomization models in engine applications, from correlations to direct numerical simulations. Oil Gas Sci Technol Revue d'IFP Energies Nouvelles 66(5):801–822. https://doi.org/10.2516/ogst/2011116

Gavaises M, Tonini S, Marchi A, Theodorakakos A, Bouris D, Matteucci L (2006) Modelling of internal and near-nozzle flow of a pintle-type outwards-opening gasoline piezo-injector. Int J Engine Res 7(5):381–397. https://doi.org/10.1243/14680874JER00306

Ghurri A, Kim J, Kim HG, Jung J, Song K (2012) The effect of injection pressure and fuel viscosity on the spray characteristics of biodiesel blends injected into an atmospheric chamber. J Mech Sci Technol 26(9):2941–2947. https://doi.org/10.1007/s12206-012-0703-1
Hiroyasu H, Arai M (1990) Structures of fuel sprays in diesel engines. SAE technical paper 900475
Kapusta ŁJ, Pielecha I, Wisłocki K, Teodorczyk A (2016) Autoignition and combustion of n-hexane spray in subcritical and supercritical environments. J Therm Anal Calorim 123(1):819–828. https://doi.org/10.1007/s10973-015-4927-z
Linstrom PJ, Mallard GW (2001) NIST chemistry WebBook, NIST Standard Reference Database Number 69. National Institute of Standards and Technology, Gaithersburg. http://webbook.nist.gov. Accessed 6 Nov 2014
Mayer WOH, Schik AHA, Vielle B, Chauveau C, Gökalp I, Talley DG, Woodward RD (1998) Atomization and breakup of cryogenic propellants under high-pressure subcritical and supercritical conditions. J Propul Power 14(5):835–842. https://doi.org/10.2514/2.5348
Oefelein JC (2006) Mixing and combustion of cryogenic oxygen-hydrogen shear-coaxial jet flames at supercritical pressure. Combust Sci Technol 178(1–3):229–252. https://doi.org/10.1080/00102200500325322
Oschwald M, Smith JJ, Branam R, Hussong J, Schik A, Chehroudi B, Talley D (2006) Injection of fluids into supercritical environments. Combust Sci Technol 178(1–3):49–100. https://doi.org/10.1080/00102200500292464
Rachedi RR, Crook LC, Sojka PE (2010) An experimental study of swirling supercritical hydrocarbon fuel jets. J Eng Gas Turbines Power 132(8):081502-1–081502-9. https://doi.org/10.1115/1.3124668
Roy A, Segal C (2010) Experimental study of fluid jet mixing at supercritical conditions. J Propul Power 26(6):1205–1211. https://doi.org/10.2514/1.48462
Schmidt V, Sender J, Oschwald M (2002) Visualization of high speed phenomena during the ignition transient of a LOX/GH2 coaxial injected spray. J Vis 5(1):3400
Segal C, Polikhov SA (2008) Subcritical to supercritical mixing. Phys Fluids. https://doi.org/10.1063/1.2912055
Shakarji CM (1998) Least-squares fitting algorithms of the NIST algorithm testing system. J Res Nat Inst Stand Technol 103(6):633. https://doi.org/10.6028/jres.103.043
Siebers DL (1999) Scaling liquid-phase fuel penetration in diesel sprays based on mixing-limited vaporization. SAE technical paper 1999-01-0528 (724). https://doi.org/10.4271/1999-01-0528
Sun C, Ning Z, Qiao X, Lv M, Fu J, Zhao J, Wang X (2018) Study of effervescent jet breakup under gas expansion disturbance. J Vis 21(6):935–948. https://doi.org/10.1007/s12650-018-0502-6
Warnecke V, Achleitner E, Bäcker H (2006) Development status of the siemens VDO piezo injection system for spray-guided combustion. In: 27th international Vienna motor symposium 2006
Zong N, Yang V (2006) Cryogenic fluid jets and mixing layers in transcritical and supercritical environments. Combust Sci Technol 178(1–3):193–227. https://doi.org/10.1080/00102200500287613